

## Reconstruction by fluorescence imaging of the spatio-temporal evolution of the viscosity field in Hele-Shaw flows

P. Bunton, B. Dice, J. A. Pojman, A. De Wit, and F. Brau

Citation: *Physics of Fluids* (1994-present) **26**, 114106 (2014); doi: 10.1063/1.4901957

View online: <http://dx.doi.org/10.1063/1.4901957>

View Table of Contents: <http://scitation.aip.org/content/aip/journal/pof2/26/11?ver=pdfcov>

Published by the [AIP Publishing](#)

---

### Articles you may be interested in

[Spatio-temporal and modal analysis of unsteady fluctuations in a high-subsonic base flow](#)

*Phys. Fluids* **26**, 086101 (2014); 10.1063/1.4891257

[Three-dimensional instabilities in a discretely heated annular flow: Onset of spatio-temporal complexity via defect dynamics](#)

*Phys. Fluids* **26**, 064102 (2014); 10.1063/1.4881435

[Two dimensional Leidenfrost droplets in a Hele-Shaw cell](#)

*Phys. Fluids* **26**, 032103 (2014); 10.1063/1.4867163

[Spatio-temporal linear stability of double-diffusive two-fluid channel flow](#)

*Phys. Fluids* **24**, 054103 (2012); 10.1063/1.4718775

[Viscous potential flow analysis of radial fingering in a Hele-Shaw cell](#)

*Phys. Fluids* **21**, 074106 (2009); 10.1063/1.3184574

---



## Reconstruction by fluorescence imaging of the spatio-temporal evolution of the viscosity field in Hele-Shaw flows

P. Bunton,<sup>1,a)</sup> B. Dice,<sup>1</sup> J. A. Pojman,<sup>2</sup> A. De Wit,<sup>3</sup> and F. Brau<sup>3,b)</sup>

<sup>1</sup>Department of Physics, William Jewell College, 500 College Hill, Liberty, Missouri 64068, USA

<sup>2</sup>Department of Chemistry, Louisiana State University, Baton Rouge, Louisiana 70803, USA

<sup>3</sup>Nonlinear Physical Chemistry Unit, Faculté des Sciences, Université libre de Bruxelles (ULB), CP231, 1050 Brussels, Belgium

(Received 27 May 2014; accepted 4 November 2014; published online 21 November 2014)

We study the spatio-temporal evolution of the viscosity field during stable and unstable radial flows of glycerol-water solutions in a horizontal Hele-Shaw cell where a localized temperature gradient is imposed. The viscosity field is reconstructed from the measurement of the fluorescence emitted by a viscosity-sensitive molecular probe (Auramine O). For an immiscible flow, the viscosity and temperature fields are obtained accurately. For miscible displacements, we show how the interplay between the viscosity changes of both fluids and the variation of the fluid thickness in the gap prevents obtaining strict quantitative reconstruction of the viscosity field. We explain how the reconstructed viscosity field can nevertheless be interpreted to obtain information about the fluid thickness and the local viscosity and temperature. © 2014 AIP Publishing LLC. [<http://dx.doi.org/10.1063/1.4901957>]

### I. INTRODUCTION

Viscous fingering (VF) instabilities impact numerous industrial and environmental applications ranging from oil recovery, CO<sub>2</sub> sequestration, pollutant dispersion, and spreading of peaks in chromatographic separation techniques to name a few. VF occurs as soon as a fluid of low viscosity, and thus high mobility, displaces another more viscous fluid in a porous medium. Control of this instability is of tantamount economic and environmental importance as a decrease of the resulting mixing between fluids by even a few percent could already yield substantial financial gains in, for example, enhanced oil recovery techniques.

As a result, interest in the control of the properties of this instability by mechanical,<sup>1–7</sup> thermal,<sup>8–13</sup> or chemical<sup>14–24</sup> ways for instance are of constant interest in the literature. Numerous experimental and theoretical works have already shown that the properties of the fingers (such as their mixing length or their area) can be strongly affected by *in situ* changes in the viscosity field distribution induced by gradients of temperature or composition in the solutions. As an example, Nagatsu *et al.* have recently shown experimentally that a chemical reaction modifying *in situ* the local value of viscosity during a reactive displacement of a viscous solution of pH-responsive polymer by a less viscous solution of a base or acid solution can modify the fingering pattern.<sup>15,20</sup> Riolfo *et al.* have furthermore evidenced that a reaction can even trigger fingering when a viscous polymer solution displaces a less viscous reactive solution.<sup>22</sup>

Qualitative understanding of the thermally- or chemically-driven control of fingering properties typically rely on numerical computation of the spatio-temporal evolution of the temperature<sup>9,12</sup> or concentrations<sup>18,21,22</sup> fields. The viscosity field is then deduced on the basis of a state equation

---

a)Electronic mail: [buntonp@william.jewell.edu](mailto:buntonp@william.jewell.edu)

b)Electronic mail: [fabian.brau@ulb.ac.be](mailto:fabian.brau@ulb.ac.be)

relating the viscosity to temperature or chemical concentrations. Alternatively, simple qualitative explanation on how the viscosity is assumed to change locally during the experiment as a function of expected changes of temperature or concentration are sometimes invoked.<sup>15</sup> At this stage, unambiguous proof that the instability mechanisms predicted theoretically are actually at play in the observed experimental pattern is however impossible. Indeed, these mechanisms rely on the local variations of some fields (temperature, concentration, or viscosity), whereas VF is typically visualized experimentally by following the spatio-temporal evolution of a dye initially mixed with one of the two fluids.<sup>8,10,15,20,22</sup> As shown numerically, the pattern of the dye is however not necessarily the same as the pattern of either the temperature, the solutes concentration, or the viscosity.<sup>21</sup> Indeed, the dye does not generally follow the same evolution equation than these other fields and its concentration remains unchanged by local gradients of temperature or composition. As a consequence, a dye does not allow to track *in situ* changes of the viscosity when a fluid passes over a local hot zone for instance or when a reaction at a miscible interface locally modifies the composition of a solute affecting the viscosity.

To understand the properties of VF and, eventually, control it by either thermal or chemical ways requires finding an alternative to follow *in situ* during an experiment the dynamic evolution of the viscosity gradients. Such an experimental access in real time to the temporal evolution of the viscosity field remains a challenge, which has not been achieved to the best of our knowledge.

In this context, we show that *in situ* quantitative analysis of the spatio-temporal evolution of the viscosity field during fluid displacements in a Hele-Shaw cell can be achieved by imaging the flow using the fluorescence emission of a viscosity-sensitive molecular probe, Auramine O.<sup>25</sup> The analysis can be applied to study both miscible and immiscible displacements in both stable and VF conditions. We show that a two-dimensional reconstruction of the dynamic viscosity field can be achieved provided the fluorescence intensity is properly calibrated with respect to the viscosity variations. While quantitative information is fairly easy to obtain in the case of immiscible fluids, the situation requires to be more cautious for miscible fluids. In this case, the nonuniform shape adopted by the injected fluid within the gap of the Hele-Shaw cell may affect the interpretation of the data. Nevertheless, comparison between relative changes of fluorescence amplitude between the displaced and injected fluids allows for studying local changes of viscosity and fluid layer thickness as demonstrated here upon visualization of local viscosity changes when the fluid passes above a locally heated region.

## II. METHOD

The system under consideration consists in a Hele-Shaw cell made of two optical quality glass plates (6 mm thick) separated by a thin gap of thickness  $b = 0.65$  mm. The cell is illuminated from above. The lower glass plate was painted with flat black paint for the fluorescence measurements and painted white for the dye measurements. Figure 1 shows a simple schematic of the experimental setup and a corresponding picture of the apparatus used for flow imaging. The injection hole is located in the center of the cell and the injection is done at a constant volume flow rate  $Q = 3.00$  ml/min with a syringe pump (See details in the Material part of Appendix C). The flow is visualized by imaging the fluorescence produced by a viscosity-sensitive molecular probe: Auramine O in this work.<sup>25</sup> The calibration is performed with water-glycerol mixture of various viscosity using a constant concentration of Auramine O, namely 0.20 mM. Therefore, in the miscible case, the concentration of the molecular probe should stay constant everywhere in the cell during the flow experiments to get meaningful results. Prior injection, both injected and displaced fluids should thus contain the same concentration of fluorescent probe, especially if the Péclet number is low.

### A. Molecular probe

Viscosity-sensitive fluorescent molecular probes are currently emerging in various fields as a powerful quantitative visualization tool. For example, they are used in polymer chemistry to study changes in free volume of polymers as a function of polymerization reaction parameters, molecular weight, and crosslinking,<sup>27–30</sup> in cell physiology to study cell membrane viscosity which is linked to

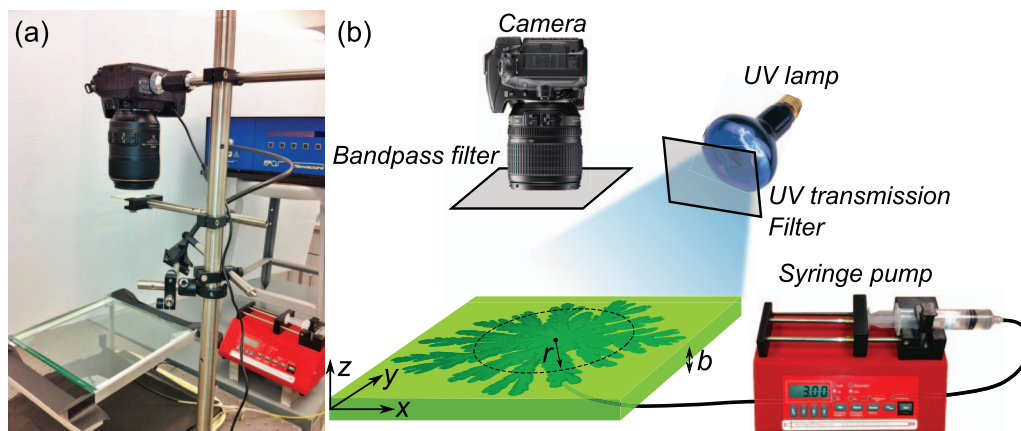


FIG. 1. (a) Photograph of imaging apparatus. (b) Schematic of imaging apparatus. The Auramine O fluorescence is induced by a 365 nm excitation light. The fluorescence is imaged with a digital camera together with a 550 nm bandpass filter. Radial pumping is accomplished with syringe pump. The distance  $b$  between the two plates of the Hele-Shaw cell is set to 0.65 mm.  $r$  is the radial distance measured from the injection point and the  $z$  coordinate is measured from the middle of the gap between the two plates.

alterations in various physiological processes in the cell<sup>31,32</sup> or in physics to measure microbubble viscosity<sup>33</sup> or to visualize shear stress in fluids.<sup>34</sup>

Auramine O, one of these fluorescent probes, belongs to the family of molecules called “molecular rotors.” Such molecules are characterized by the ability to form, upon photoexcitation, twisted intramolecular charge transfer (TICT) states through the rotation of one segment of the structure with respect to the rest of the molecule.<sup>35</sup> After photon absorption, a molecular rotor can return to the ground state either from the locally excited state (planar state) or from the twisted state. In the first case, the excited electron relaxes to a number of vibrational states and loses energy before returning to the ground state through photoemission (Fig. 2). This loss of energy through vibrational states is predominantly responsible for the wavelength shift between absorption and fluorescence spectra (Fig. 3(a)). The fluorescence lifetime for Auramine O is smaller than 130 ps<sup>36,37</sup> which ensure an essentially instantaneous response time compared to the typical hydrodynamic timescale of the experiments. In the second case, the molecule is excited to a TICT state and returns to the ground state through (nonradiative) vibrational relaxation because of the low TICT  $S_1 - S_0$  energy gap (Fig. 2). Notice that some molecular rotors have a larger TICT  $S_1 - S_0$  energy gap, such as DMABN,<sup>38</sup> and emit radiation to relax to the ground state yielding dual emission bands.

In order to reach a TICT state from the locally excited state, the electron needs to pass over a potential barrier,  $\Delta(\mu)$  (Fig. 2). This energy gap is influenced by the interaction with the molecules of the solvent through dipole-dipole interactions, hydrogen bonds, isomerization, or excimer formation. This potential barrier is also sensitive to steric hindrance and increases with the solvent bulk viscosity.<sup>35,39</sup> The probability of energy relaxation through the TICT state is then reduced as the solvent viscosity increases and radiative relaxation is thus favored leading to an increase of the fluorescence intensity. This effect is shown in Fig. 3(b) giving the fluorescence intensity of 0.20 mM of Auramine O in water-glycerol solutions measured for various mass concentration of glycerol using a spectrometer equipped with the same bandpass filter as used with our camera. The viscosity-dependent fluorescence is characterized by a broad band between 500 nm and 600 nm peaking around 510–520 nm (see Fig. 3(a)).<sup>40</sup> The excitation spectrum is predominately located between 350 nm and 470 nm and produces the same fluorescence spectrum when the wavelength of the excitation light spans this interval.

These spectra could in principle be used to obtain a calibration curve relating fluorescence intensities to viscosity. However, the experiments are imaged in a different geometry using a camera instead of the spectrometer. We thus used another procedure to obtain the calibration curve as explained hereafter.

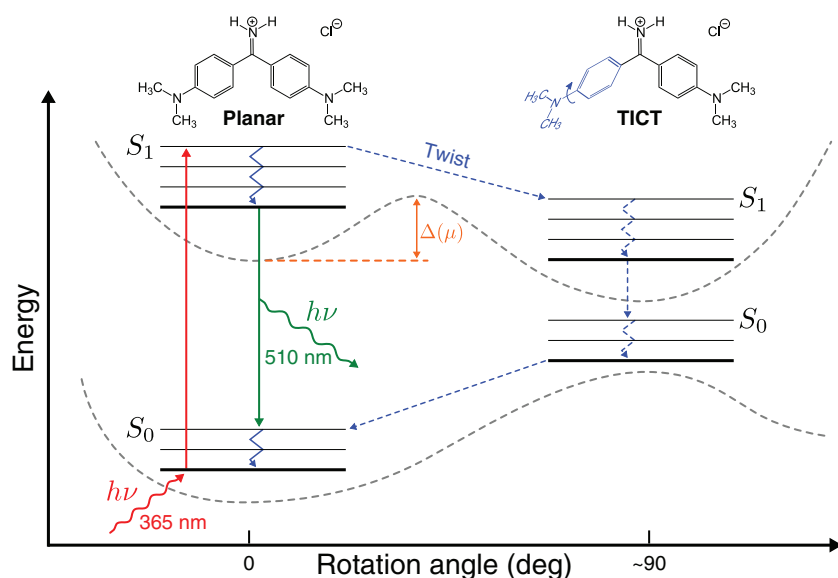


FIG. 2. Schematic Jablonski diagram of the molecular rotor Auramine O. Solid downward arrows indicate a relaxation from a locally excited state leading to fluorescence, whereas dashed arrows indicate a nonradiative relaxation through a TICT state (the rotation angle is about  $86^\circ$  for Auramine O<sup>26</sup>). The upward (red) and downward (green) solid arrows represent the photon absorption and emission, respectively. Broken arrows (blue) indicate nonradiative relaxation. The excitation wavelength used in our experiments is indicated as well as the typical emission wavelength for Auramine O. The dashed curves (gray) represent idealized potential energy for planar and twisted ground ( $S_0$ ) and excited ( $S_1$ ) states.

## B. Calibration

The calibration of the fluorescence intensity as a function of fluid viscosity is performed as follows. The Hele-shaw cell is filled by various water-glycerol mixtures of known viscosity<sup>41</sup> containing the same concentration of Auramine O, namely 0.20 mM. Images of the cell filled with various water-glycerol mixtures of known composition are taken with a camera equipped with a 550 nm filter and located above the cell, while the experimental setup is in complete dark to measure the spurious background light,  $I_B$ . The cell is then illuminated from above by a 365 nm excitation light and images are taken to measure the fluorescence intensity  $I_{WG}$ . The background light  $I_B$  is then subtracted from these images. The image obtained when the cell is filled by pure glycerol is used as reference for fluorescence intensity,  $I_0$ . For other compositions, the grayscale values  $I_{WG}$  of each pixel of each image are then divided by the grayscale value of this reference image to obtain relative

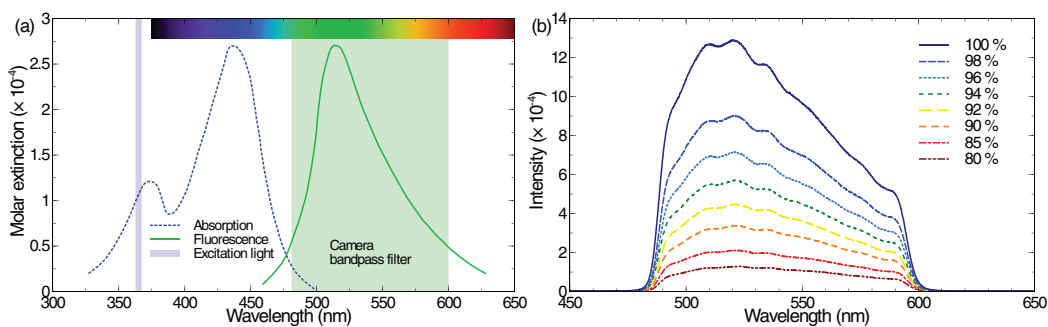


FIG. 3. (a) Absorption and fluorescence spectra of Auramine O in glycerol at  $25^\circ\text{C}$  (data from Ref. 40). The relevant wavelengths for the excitation light and the camera filter are also indicated. (b) Fluorescence spectra of 0.20 mM of Auramine O in water-glycerol solutions at  $20^\circ\text{C}$  for various mass concentration of glycerol. The solutions were placed inside a cuvette and the spectra were measured by a spectrometer using the same bandpass filter as during the flow experiments.

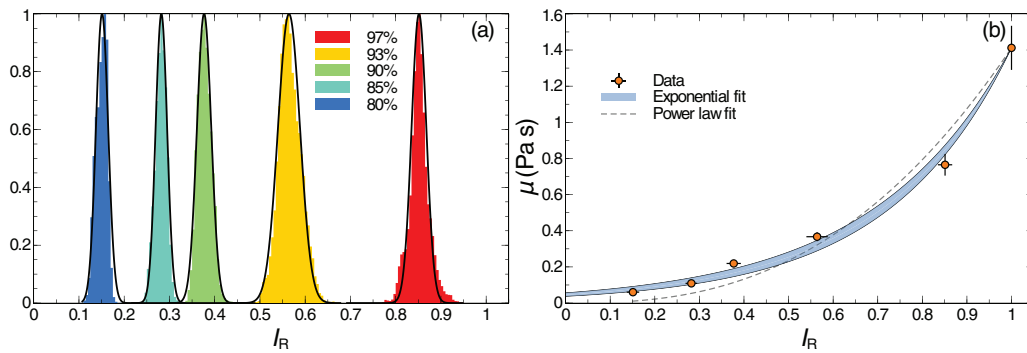


FIG. 4. (a) Distributions of the relative fluorescence intensity,  $I_R$ , over the cell filled by aqueous solutions of glycerol with various concentrations. The distributions are arbitrarily normalized to 1. A gaussian fit is used to estimate the errors on  $I_R$ . (b) Evolution of the viscosity of the water-glycerol solutions as a function of  $I_R$ . The horizontal error bars are due to the finite width of the distributions shown in panel (a) and the vertical error bars are obtained by assuming an error of 1 °C in the temperature of the solutions. The data are fitted by the exponential law (2). The shaded area corresponds to the region spanned when the fitting parameter varies over one standard deviation.

fluorescence intensities,  $I_R$ . For each pixel, we thus apply the following formula:

$$I_R = \frac{I_{WG} - I_B}{I_0 - I_B}. \quad (1)$$

The distributions of these relative intensities over each image are shown in Fig. 4(a). They are fitted by Gaussian functions to estimate their width, which gives the errors on  $I_R$ . The relation between the viscosity of each water-glycerol mixture and the fluorescence intensities obtained by this procedure is shown in Fig. 4(b). The vertical error bars are obtained by assuming an error of 1 °C on the water-glycerol mixture temperature. A one-parameter exponential fit describes well the data over the range of fluorescence intensities considered in this work:

$$\mu = \mu_g e^{B(I_R - 1)}, \quad (2)$$

where  $\mu_g = 1412$  mPa s is the pure glycerol viscosity at room temperature (20 °C) and  $B = 3.43 \pm 0.21$  is the fitting parameter.

This calibration curve relates the fluid viscosity,  $\mu$ , to the relative fluorescence intensity,  $I_R$ , and allows thus to reconstruct *in situ* and in real time values of the local viscosity during Hele-Shaw flows. For this purpose, we use Eq. (1) for each pixel where we replace  $I_{WG}$  by the fluorescence intensity of this pixel in the grayscale flow image,  $I_F$ ,

$$I_R = \frac{I_F - I_B}{I_0 - I_B}. \quad (3)$$

### III. SPATIO-TEMPORAL EVOLUTION OF THE VISCOSITY FIELD

In order to illustrate the physical insights gained thanks to tracking the local viscosity field, we have performed several displacement experiments using a thermoelectric heater localized in a small region below the cell. The objective is to induce locally some viscosity changes due to a local heating and analyze the related two-dimensional viscosity field quantitatively reconstructed using a fluorescence probe. Initially, the horizontal cell is filled by a fluid of viscosity  $\mu_2$  which is then displaced radially by another fluid of viscosity  $\mu_1$ . If  $\mu_1 > \mu_2$ , the displacement is viscously stable and gives a circle expanding radially and deformed locally in the zone where the localized heating favors increased flow. If  $\mu_1 < \mu_2$ , a viscous fingering instability takes place leading to a fingered-shape deformation of the interface.<sup>42</sup> In Sec. III A, we consider displacements of immiscible fluids whereas miscible displacements are discussed in Sec. III B. The viscosity field is reconstructed from both the relative fluorescence intensity maps (3) and the calibration curve (2). These results are

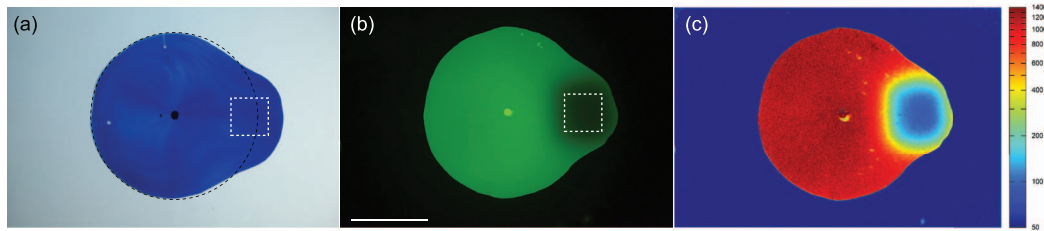


FIG. 5. Pure glycerol displacing air at  $t = 150$  s with a localized hot region. (a) Visualization with the help of the non-fluorescent trypan blue dye. (b) Visualization using Auramine O. (c) Reconstructed viscosity field (mPa s) in logarithmic scale using Eq. (3) together with the calibration curve (2). The scale bar corresponds to 5 cm and the white dashed squares show the position of the thermoelectric heater.

compared to those obtained using non-fluorescent dyes (simply denoted dye in the following), such as trypan blue, for visualizing the flow.

### A. Immiscible case

During a Hele-Shaw flow involving two immiscible fluids, the interface is sharp, and the viscosity on both sides is constant and equal to the initial viscosity of each fluid. In order to induce a viscosity gradient, a thermoelectric heater is placed below the cell and produces locally a temperature gradient. Near this heat source, the fluid viscosity decreases and the fluid volume expands which leads to a deformation of the interface. In the stable case, when pure glycerol is injected into air (Fig. 5), the interface is no longer circular and bulges toward the hot region. When visualized with a dye (Fig. 5(a)), only information about the shape of the interface is accessible. In contrast, using Auramine O as a probe allows visualization of the viscosity gradient inside the injected glycerol (Fig. 5(b)). The reconstructed viscosity field is shown in Fig. 5(c).

### B. Miscible case

During a Hele-Shaw flow involving two miscible fluids, mixing occurs at the contact zone between them producing a viscosity gradient. However, the Péclet number of our experiment is rather large ( $Pe = Q/(bD) \gtrsim 10^5$ , where  $D$  is the diffusion coefficient) and diffusion is negligible compared to advective transport. The interface can thus be considered as sharp in good approximation with a constant viscosity on both sides of the interface as for immiscible fluids. However, the fluorescence intensity measured during the flow experiments presents a smooth gradient between the two fluids (see Fig. 6(b) which contrasts with Fig. 5(b) where the interface is sharp). This fluorescence gradient is due to the Poiseuille-like shape adopted by the injected fluid within the cell gap because of the absence of surface tension. Using a sharp interface as approximation, it is possible to relate  $I_R$  to this 3D shape as explained in Appendix A.

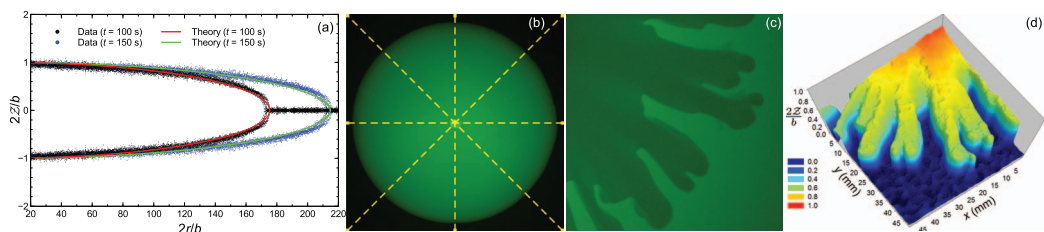


FIG. 6. (a) Radial profiles of the stable displacement obtained with pure glycerol containing 0.20 mM of Auramine O displacing pure glycerol without Auramine O at  $t = 100$  s and  $t = 150$  s. Data are collected along 8 radial lines with an angular distance of  $\pi/4$  as shown in panel (b). The theoretical profiles (B14) are also displayed on (a) as solid lines. (c) Zoom with field view of 48 mm  $\times$  48 mm of a viscously unstable displacement of pure glycerol by an aqueous glycerol solution (glycerol mass concentration of 85%) at  $t = 100$  s. (d) 3D reconstruction of the fingers using Eq. (A3) in Appendix A.

To highlight the physical insight gained in the dynamics by the use of fluorescence, we first consider the stable situation where pure glycerol containing 0.20 mM of Auramine O displaces pure glycerol without Auramine O. As stated above, the concentration of Auramine O should ideally be constant everywhere over the cell to get consistent results with respect to calibration, which is not the case in this experiment. However, since we are working at high Péclet number, mixing due to diffusion is negligible and one can assume with good accuracy that the concentration of Auramine O inside the injected fluid remains constant during the experiment timescale. In this situation, the shape adopted by the injected fluid can be computed exactly using the Stokes approximation (creeping flow), since the Reynolds number characterizing our experiments is low ( $Re \lesssim 10^{-4}$ ). This exact expression is given by Eq. (B14) in Appendix B. The relative fluorescence intensity is measured along eight radial lines separated by an angular distance of  $\pi/4$  as shown in Fig. 6(b). The experimental shape of the injected fluid is reconstructed from the relative fluorescence intensity using Eq. (A3) with  $I_R(\mu_2) = 0$  (because there is no Auramine O in the displaced fluid) and  $I_R(\mu_1) = 1$  (because the injected fluid is pure glycerol). The result is reported in Fig. 6(a). The data dispersion is due in part to the slight departure from perfect radial symmetry. The agreement between experimental and theoretical shapes is good and shows that a quantitative measurement of the characteristics of the flow can be obtained. The same procedure can be applied to reconstruct the 3D profile of the injected fluid in the unstable situation where a less viscous fluid displaces a more viscous one. In the previous stable case, it was not possible to dissolve the molecular probe in both fluids because they are identical and would thus produce the same fluorescence intensity making them indistinguishable. In present unstable case, both fluids contain the same concentration of Auramine O and produce different fluorescence intensities due to the viscosity contrast. Figure 6(c) shows the fluorescence intensity and Fig. 6(d) shows the 3D spatial reconstruction of fingers of the injected water-glycerol solution displacing pure glycerol.

The results summarized in Fig. 6 could in principle be obtained with dyes using a procedure similar to the one explained in Ref. 43. However, imaging via a dye does not allow to track the viscosity gradients behind the dye/colorless interface within the mixing zone. Indeed, once a thermoelectric heater is placed below the cell and induces a viscosity gradient, a visualization based on dyes does not provide physical insight on the dynamics beyond the 3D shape of the flow as shown in Figs. 7(a) and 7(d). The inset of Fig. 7(a) shows the relative grayscale intensity obtained

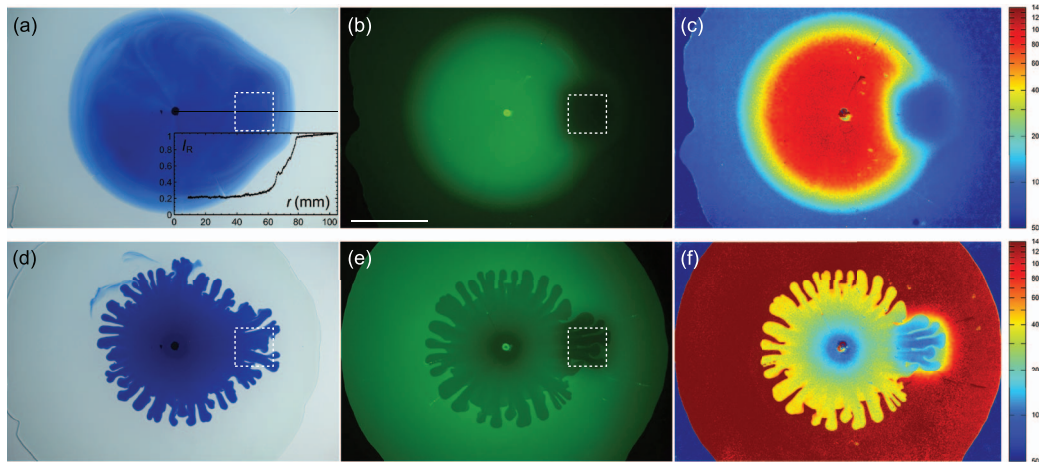


FIG. 7. (a)–(c). Pure glycerol displacing a water-glycerol solution (glycerol mass concentration of 85%) at  $t = 150$  s with a localized hot region. (a) Visualization with the help of non-fluorescent dye. (b) Visualization using Auramine O. (c) Reconstructed viscosity field (mPa s) in logarithmic scale using Eq. (3) together with the calibration curve (2). Inset panel (a): relative grayscale intensity obtained by dividing the gray value of each pixel of the photo a by the gray value of the photo taken just before injection. (d)–(f) Water-glycerol solution (glycerol mass concentration of 85%) displacing pure glycerol at  $t = 70$  s with a localized hot region. (d) Visualization with the help of non-fluorescent dye. (e) Visualization using Auramine O. (f) Reconstructed viscosity field (mPa s) in logarithmic scale using Eq. (3) together with the calibration curve (2). The scale bar corresponds to 5 cm and the white dashed squares show the position of the thermoelectric heater.

by dividing the gray value of each pixel of Fig. 7(a) by the gray value of the photo taken just before injection. This relative intensity profile is related to the actual 3D profile of the injected fluid and shows a smooth transition between the two fluids due to the Poiseuille-like profile. On the contrary, when using a fluorescent probe, local changes in viscosity can already be tracked by fluorescence intensity changes as shown in Figs. 7(b) and 7(e). The reconstructed viscosity fields shown in Figs. 7(c) and 7(f) provide new physical information compared to dye visualization with a strong viscosity gradient near the hot region.

To show this, let us first note that the fluorescence intensity is influenced by both the 3D shape of the injected fluid and the viscosity gradient. Consequently, the numbers in the color scale of Figs. 7(c) and 7(f) must be used for interpretation of the data by taking these two elements into account. Indeed, far from the heater, the variation of fluorescence intensity is essentially due to the thickness variation of the layer of injected fluid as shown in Fig. 6. Near the heater, the change of fluorescence intensity is in contrast essentially due to the variation of the viscosity of both injected and displaced fluids since, in this small region, the thickness modulation is moderate.

These effects are well seen in Fig. 7(f). Near the injection point, the thickness of the injected fluid layer is almost equal to the cell gap. The reconstructed viscosity field is low and equals the viscosity of the less-viscous injected fluid. In contrast, the fingers located far from the heat source appear with an intermediate viscosity not because the viscosity has increased but because the thickness of the injected fluid is also intermediate. Indeed, the relative fluorescence intensity is  $I_R \simeq 0.65$  in these regions (which, through Eq. (2), implies  $\mu \simeq 425$  mPa s in the scale of Fig. 7(f)). If we again assume that there is no significant mixing between the two fluids because of the high value of the Péclet number, Eq. (A3) gives the thickness of these fingers. The viscosity of the injected fluid<sup>41</sup> is  $\mu_1 = 109$  mPa s which corresponds to  $I_R(\mu_1) \simeq 0.25$  from Eq. (2). Since the displaced fluid is pure glycerol, we have  $I_R(\mu_2) \simeq 1$ . Therefore, Eq. (A3) gives  $2Z/b \simeq 0.47$  meaning that the fingers fill half of the cell gap. Above the source of heat, the reconstructed viscosity appears low because the viscosity of each fluid is reduced by the increase in temperature. Indeed, the regions between the fingers are occupied solely by the displaced fluid, and we measured there  $I_R = I_R(\mu_2) \simeq 0.43$ . From Eq. (2) this implies  $\mu_2 \simeq 200$  mPa s leading to a temperature of about 45 °C according to Ref. 41. Inside the fingers, we measured  $I_R \simeq 0.25$ . If we assume that the finger thickness is not significantly affected by the increase in temperature ( $2Z/b \simeq 0.47$ ), Eq. (A2) gives then  $I_R(\mu_1) \simeq 0.063$  leading to  $\mu_1 = 54$  mPa s. This corresponds to a temperature of about 30 °C inside the fingers located above the heat source. If we assume that the thickness of the fingers increases, for instance, by 10% due to thermal expansion, the viscosity slightly increases up to  $\mu_1 = 60$  mPa s leading to roughly the same estimation for the temperature.

The interplay between the viscosity changes of both fluids and the variation of fluid thickness prevents obtaining strict quantitative reconstruction of the viscosity field for miscible fluids. Nevertheless, (semi-)quantitative information can still be obtained, as shown here. In particular, local values of temperature and of liquid layer thickness can be computed. This relative quantitative information should prove to be important for non-ideal mixing or when products with viscosities larger or smaller than the injected and displaced fluids are formed at the contact zone in reactive displacements. Notice that using the 3D profile obtained with a non-fluorescent dye together with results obtained from fluorescence intensity should allow one to refine the information about the viscosity field.

#### IV. CONCLUSIONS

Results shown herein demonstrate that real-time quantitative determination of the viscosity field can be achieved from the fluorescence of a molecular probe during stable displacements and viscous fingering of both miscible and immiscible fluids for sufficiently high values of viscosity. We show that, for immiscible displacements, fluorescence measurement allows for a quantitative reconstruction of the viscosity field even in regions where changes due to a local heating cannot be tracked by the use of a dye. For miscible fluids, the local value of viscosity during displacements in Hele-Shaw cells depends on both the thickness of the injected fluid layer and temperature. We are able here to reconstruct from fluorescence the relative weight of each effect in the various regions

of the flow. This provides physical information on the spatio-temporal distribution of viscosity, film thickness, and temperature during fingering in the Hele-Shaw cell influenced by a local heating.

The primary limitations of the analysis are the noise, limited sensitivity, and intensity resolution of the camera as well as the stability of the excitation lamp. Use of a scientific-grade, cooled CCD array camera should vastly increase the sensitivity to the emitted fluorescence leading to more subtle gradients in viscosity. Insight into the nonlinear dynamics of viscous fingering gained by our analysis should be easily transferable to a variety of displacement problems with the primary limitation being the existence of a sufficiently soluble, viscosity-sensitive molecular probe in the liquids of interest.

## ACKNOWLEDGMENTS

We thank S. Stewart and G. Brooks for assisting with the experiments. We thank Q. Tran-Cong-Miyata of the Kyoto Institute of Technology for suggesting Auramine O as the appropriate molecular probe for this study. P.B. acknowledges this work was supported by the National Science Foundation under Grant No. CBET-1335739. A.D. and F.B. thank Prodex and the FRS-FNRS Forecast programme for financial support.

## APPENDIX A: RELATION BETWEEN 3D PROFILES AND FLUORESCENCE INTENSITY FOR MISCIBLE DISPLACEMENTS

### 1. Hele-Shaw cell containing one fluid

Let us first consider the simple case where the Hele-Shaw cell contains only one fluid. In that case, the fluorescence intensity is constant over the cell and is only a function of the viscosity of the fluid. A relation can thus be obtained between the viscosity and the fluorescence intensity.

Let  $I_\mu$  denotes the intensity of fluorescence per unit volume emitted by a fluid of viscosity  $\mu$ . Let  $S$  be the area seen on 1 image pixel. If one neglects the absorption by the fluid of the emitted light, the fluorescence intensities received by this pixel is simply the sum of the intensities emitted by each elementary fluid volume below the area  $S$ . The relative fluorescence intensity,  $I_R$ , of that pixel with respect to a fluid of reference with viscosity  $\mu_0$  (pure glycerol in our case) is thus given by

$$I_R(\mu) = \frac{\int dS \int_{-\frac{b}{2}}^{\frac{b}{2}} I_\mu dz}{\int dS \int_{-\frac{b}{2}}^{\frac{b}{2}} I_{\mu_0} dz} = \frac{I_\mu}{I_{\mu_0}}. \quad (\text{A1})$$

The relation we obtain between  $I_R$  and the viscosity  $\mu$  is given in Eq. (2).

### 2. Hele-Shaw cell containing one fluid displacing another fluid

At high enough Péclet numbers, and for miscible displacements, the measured fluorescence intensity is dominated by the 3D shape of the injected fluid and the diffusion between the two miscible fluids plays a minor role. Consequently, the contact area between the two fluids can be considered as being sharp in good approximation. Moreover, if the two fluids are not reactive and if there is no temperature gradient, the viscosity is thus constant in each region separated by this sharp interface. The variation of fluorescence intensity is thus due to the 3D shape of the injected fluid.

The situation described here is illustrated by Fig. 8 where a cross-section shows that the slightly diffuse interface between the two fluids is approximated by a sharp interface,  $\mathcal{Z}(r, \theta, t)$ . The 3D profile of the injected fluid can be reconstructed once the relation between  $\mathcal{Z}(r, \theta, t)$  and the relative fluorescence intensity measured experimentally is known. To derive this relation, we neglect the difference of density between the injected and the displaced fluid. We thus assume that the shape of the injected fluid is symmetric with respect to the plane  $z = 0$ .

The fluorescence intensity received by 1 image pixel is still given by the sum of the intensities emitted by each elementary fluid volume below the area  $S$ . However, these intensities vary now along the vertical direction  $z$ . The relative fluorescence intensity,  $I_R$ , of that pixel with respect to the

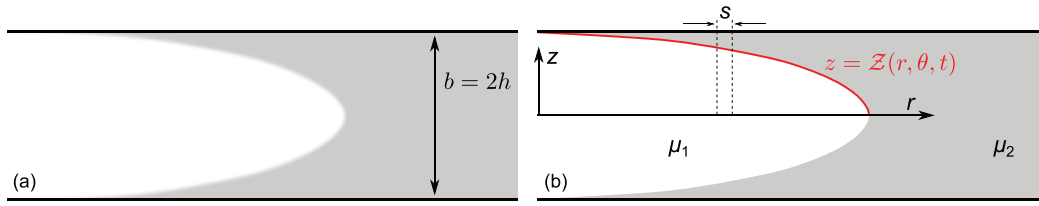


FIG. 8. (a) Schematic Poiseuille-like profile at large Péclet numbers of a fluid of viscosity  $\mu_1$  displacing another fluid of viscosity  $\mu_2$  between two parallel plates separated by a small gap  $b = 2h$ . (b) Sharp interface idealization and definition of  $\mathcal{Z}$ .

same fluid of reference with viscosity  $\mu_0$  is then given by

$$\begin{aligned} I_R(r, \theta, t) &= \frac{\int dS \left[ \int_{-\frac{b}{2}}^{-\mathcal{Z}} I_{\mu_2} dz + \int_{-\mathcal{Z}}^{\mathcal{Z}} I_{\mu_1} dz + \int_{\mathcal{Z}}^{\frac{b}{2}} I_{\mu_2} dz \right]}{\int dS \int_{-\frac{b}{2}}^{\frac{b}{2}} I_{\mu_0} dz} = \frac{I_{\mu_1} 2\mathcal{Z}(r, \theta, t)}{I_{\mu_0} b} + \frac{I_{\mu_2}}{I_{\mu_0}} \left( 1 - \frac{2\mathcal{Z}(r, \theta, t)}{b} \right), \\ &= I_R(\mu_1) \frac{2\mathcal{Z}(r, \theta, t)}{b} + I_R(\mu_2) \left( 1 - \frac{2\mathcal{Z}(r, \theta, t)}{b} \right), \end{aligned} \quad (\text{A2})$$

where we introduced the quantities  $I_R(\mu)$  defined in Eq. (A1) and measured during the calibration process. Notice that we have also assumed that  $S$  is small enough such as  $\mathcal{Z}(r, \theta, t)$  can be considered as constant over this area. The profile is thus approximated by a piecewise constant function which is a consequence of the finite resolution of the camera. Finally, the relation between the 3D profile of the injected fluid,  $\mathcal{Z}(r, \theta, t)$ , and the measured relative fluorescence intensity,  $I_R(r, \theta, t)$ , is thus given by

$$\frac{2\mathcal{Z}(r, \theta, t)}{b} = \frac{I_R(r, \theta, t) - I_R(\mu_2)}{I_R(\mu_1) - I_R(\mu_2)}. \quad (\text{A3})$$

## APPENDIX B: LAMINAR RADIAL FLOW BETWEEN TWO PARALLEL PLATES

We recall the derivation of the exact solution of the velocity profile, obtained using the Stokes approximation, for a laminar radial flow confined between two parallel plates. As shown below, this approximation is suitable in our case (provided both fluids have the same viscosity) since we are working at very low Reynolds number ( $Re \lesssim 10^{-4}$ ). Discussions about extensions of this solution including inertial effects and comparison to experiments at large Reynolds number can be found, for example, in Refs. 44–49.

The solution to the Navier-Stokes equation presented here can be found, for example, in Refs. 45 and 50 and is reproduced here for completeness. The Navier-Stokes equations for incompressible fluids reads

$$\partial_t \mathbf{v} + (\mathbf{v} \cdot \nabla) \mathbf{v} = -\frac{\nabla P}{\rho} + \frac{\mu}{\rho} \nabla^2 \mathbf{v}, \quad (\text{B1})$$

together with

$$\nabla \cdot \mathbf{v} = 0, \quad (\text{B2})$$

where  $\mu$  is the dynamic viscosity and  $\rho$  is the mass density. Using cylindrical coordinates  $(r, \theta, z)$ , assuming radial symmetry with  $\mathbf{v} = (v_r, 0, 0)$ ,  $v_r = v_r(r, z, t)$ , and  $\partial_\theta P = 0$ , the radial component of Eq. (B1) reads

$$\partial_t v_r + v_r \partial_r v_r = -\frac{1}{\rho} \partial_r P + \frac{\mu}{\rho} \left( \partial_r^2 v_r + \partial_z^2 v_r + \frac{1}{r} \partial_r v_r - \frac{v_r}{r^2} \right). \quad (\text{B3})$$

The  $\theta$ -component of Eq. (B1) yields an identity and the  $z$ -component is given by

$$\partial_z P = 0. \quad (\text{B4})$$

Consequently, the pressure depends only on the radial coordinate and time,  $P = P(r, t)$ . The continuity equation (B2) leads to

$$\frac{1}{r} \partial_r (r v_r) = \partial_r v_r + \frac{v_r}{r} = 0. \quad (\text{B5})$$

Using the continuity equation (B4), the Navier-Stokes equation (B3) reduces to

$$\partial_t v_r - \frac{v_r^2}{r} = -\frac{1}{\rho} d_r P + \frac{\mu}{\rho} \partial_z^2 v_r. \quad (\text{B6})$$

A steady velocity profile for Stokes flow (neglecting the nonlinear term) is then solution of the following:

$$\mu \partial_z^2 v_r = d_r P, \quad (\text{B7})$$

which is readily integrated with the no-slip boundary condition ( $v_r(r, \pm h) = 0$ , where  $b = 2h$  is the gap width) to give

$$v_r = \frac{1}{2\mu} d_r P (z^2 - h^2). \quad (\text{B8})$$

Volume conservation leads to the relation

$$Q = 2 \int_0^h 2\pi r v_r dz, \quad (\text{B9})$$

which gives the pressure profile

$$d_r P = -\frac{3\mu Q}{4\pi h^3 r}. \quad (\text{B10})$$

The radial velocity profile is thus given by

$$v_r = \frac{3Q}{8\pi h^3 r} (z^2 - h^2). \quad (\text{B11})$$

At this stage, we can estimate the error introduced by the Stokes approximation by looking under which condition we have

$$\mu \partial_z^2 v_r \gg \max_{z \in [-h, h]} \rho \frac{v_r^2}{r}. \quad (\text{B12})$$

Using Eq. (B11), we find that this condition is equivalent to

$$\frac{r}{h} \gg \left( \frac{3Q\rho}{16\pi\mu h} \right)^{1/2} \simeq 0.09. \quad (\text{B13})$$

In our case, as  $b = 2h = 0.65$  mm, this is still equivalent to  $r \gg 30 \mu\text{m}$  which is obviously satisfied. Finally, the 3D profile adopted by the injected fluid is given by the following ODE:

$$v_r = d_t r = \frac{3Q}{8\pi h^3 r} (z^2 - h^2), \quad (\text{B14})$$

whose solution can be written as

$$\frac{\bar{r}^2}{\bar{t}} + \bar{z}^2 = 1, \quad (\text{B15})$$

with  $\bar{r} = r/h$ ,  $\bar{z} = z/h$ ,  $\bar{t} = t/T$ , and  $T = 4\pi h^3/3Q$ . This is the equation of an ellipse centred at the origin of the coordinates and whose radius along the  $r$ -axis grows as  $\sqrt{t}$ , whereas the radius along the  $z$ -axis stays constant in time and equal to  $h = b/2$ .

## APPENDIX C: MATERIAL

Fluorescence imaging is performed using a Nikon D7000 camera together with a Sigma DC 18–50 mm 1:2.8–4.5 HSM lens. The camera settings for fluorescence imaging are  $f/4.5$ ,  $1/4$  s exposure, and ISO 3200. An Ocean Thin Films BPF 550 nm filter providing a bandpass of nominally 500–600 nm is placed in front of the camera. A 365 nm excitation light is provided by an EFOS Novacure lamp with fluid-filled light guide. Both the internal 365 nm filter in the light source and a Schott UG-11 UV filter are used to filter the output of the light guide. Radial pumping is accomplished with a New Era Pump Systems Model NE-300 syringe pump. Auramine O was purchased from Aldrich. Glycerol from Fisher Scientific is certified ACS grade, 99.5% purity. An Acton Research 0.3 m spectrometer was used to measure the fluorescence spectra of Auramine O for various compositions of water-glycerol mixtures.

- <sup>1</sup> S. W. Li, J. S. Lowengrub, J. Fontana, and P. Palffy-Muhoray, “Control of viscous fingering patterns in a radial Hele-Shaw cell,” *Phys. Rev. Lett.* **102**, 174501 (2009).
- <sup>2</sup> D. Pihler-Puzovic, P. Illien, M. Heil, and A. Juel, “Suppression of complex fingerlike patterns at the interface between air and a viscous fluid by elastic membranes,” *Phys. Rev. Lett.* **108**, 074502 (2012).
- <sup>3</sup> E. O. Dias, E. Alvarez-Lacalle, M. S. Carvalho, and J. A. Miranda, “Minimization of viscous fluid fingering: A variational scheme for optimal flow rates,” *Phys. Rev. Lett.* **109**, 144502 (2012).
- <sup>4</sup> T. T. Al-Housseiny, P. A. Tsai, and H. A. Stone, “Control of interfacial instabilities using flow geometry,” *Nat. Phys.* **8**, 747–750 (2012).
- <sup>5</sup> D. Pihler-Puzovic, R. Périllat, M. Russell, A. Juel, and M. Heil, “Modelling the suppression of viscous fingering in elastic-walled Hele-Shaw cells,” *J. Fluid Mech.* **731**, 162–183 (2013).
- <sup>6</sup> T. T. Al-Housseiny and H. A. Stone, “Controlling viscous fingering in tapered Hele-Shaw cells,” *Phys. Fluids* **25**, 092102 (2013).
- <sup>7</sup> E. O. Dias and J. A. Miranda, “Taper-induced control of viscous fingering in variable-gap Hele-Shaw flows,” *Phys. Rev. E* **87**, 053015 (2013).
- <sup>8</sup> K. E. Holloway and J. R. de Bruyn, “Viscous fingering with a single fluid,” *Can. J. Phys.* **83**, 551–564 (2005).
- <sup>9</sup> K. E. Holloway and J. R. de Bruyn, “Numerical simulations of a viscous fingering instability in a fluid with a temperature-dependent viscosity,” *Can. J. Phys.* **84**, 273–287 (2006).
- <sup>10</sup> Y. Nagatsu, N. Fujita, Y. Kato, and Y. Tada, “An experimental study of non-isothermal miscible displacements in a Hele-Shaw cell,” *Exp. Therm. Fluid Sci.* **33**, 695–705 (2009).
- <sup>11</sup> M. N. Islam and J. Azaiez, “Miscible thermo-viscous fingering instability in porous media: Part 1: Linear stability analysis,” *Transp. Porous Med.* **84**, 821–844 (2010).
- <sup>12</sup> M. N. Islam and J. Azaiez, “Miscible thermo-viscous fingering instability in porous media: Part 2: Numerical simulations,” *Transp. Porous Med.* **84**, 845–861 (2010).
- <sup>13</sup> A. Tran-Viet, A. F. Routh, and A. W. Woods, “Control of the permeability of a porous media using a thermally sensitive polymer,” *AIChE J.* **60**, 1193–1201 (2014).
- <sup>14</sup> T. Podgorski, M. C. Sostarecz, S. Zorman, and A. Belmonte, “Fingering instabilities of a reactive micellar interface,” *Phys. Rev. E* **76**, 016202 (2007).
- <sup>15</sup> Y. Nagatsu, K. Matsuda, Y. Kato, and Y. Tada, “Experimental study on miscible viscous fingering involving viscosity changes induced by variations in chemical species concentrations due to chemical reactions,” *J. Fluid Mech.* **571**, 475–493 (2007).
- <sup>16</sup> S. Swernath and S. Pushpavanam, “Viscous fingering in a horizontal flow through a porous medium induced by chemical reactions under isothermal and adiabatic conditions,” *J. Chem. Phys.* **127**, 204701 (2007).
- <sup>17</sup> T. Gérard and A. De Wit, “Miscible viscous fingering induced by a simple  $A+B \rightarrow C$  chemical reaction,” *Phys. Rev. E* **79**, 016308 (2009).
- <sup>18</sup> S. H. Hejazi, P. M. J. Trevelyan, J. Azaiez, and A. De Wit, “Viscous fingering of a miscible reactive  $A+B \rightarrow C$  interface: A linear stability analysis,” *J. Fluid Mech.* **652**, 501–528 (2010).
- <sup>19</sup> S. H. Hejazi and J. Azaiez, “Hydrodynamic instability in the transport of miscible reactive slices porous media,” *Phys. Rev. E* **81**, 056321 (2010).
- <sup>20</sup> Y. Nagatsu, C. Iguchi, K. Matsuda, Y. Kato, and Y. Tada, “Miscible viscous fingering involving viscosity changes of the displacing fluid by chemical reactions,” *Phys. Fluids* **22**, 024101 (2010).
- <sup>21</sup> Y. Nagatsu and A. De Wit, “Viscous fingering of a miscible reactive  $A + B \rightarrow C$  interface for an infinitely fast chemical reaction: Nonlinear simulations,” *Phys. Fluids* **23**, 043103 (2011).
- <sup>22</sup> L. A. Riolfo, Y. Nagatsu, S. Iwata, R. Maes, P. M. J. Trevelyan, and A. De Wit, “Experimental evidence of reaction-driven miscible viscous fingering,” *Phys. Rev. E* **85**, 015304(R) (2012).
- <sup>23</sup> S. M. Davison, H. Yoon, and M. J. Martinez, “Pore scale analysis of the impact of mixing-induced reaction dependent viscosity variations,” *Adv. Water Resour.* **38**, 70–80 (2012).
- <sup>24</sup> T. I. Burghelca and I. A. Frigaard, “Unstable parallel flows triggered by a fast chemical reaction,” *J. Non-Newtonian Fluid Mech.* **166**, 500–514 (2011).
- <sup>25</sup> *Industrial Dyes: Chemistry, Properties, Applications*, edited by K. Hunger (Wiley-VCH, 2003).
- <sup>26</sup> C. Singh, B. Modak, J. A. Mondal, and D. K. Palit, “Ultrafast twisting dynamics in the excited state of auramine,” *J. Phys. Chem. A* **115**, 8183–8196 (2011).
- <sup>27</sup> R. O. Loutfy, “Fluorescence probes for polymer free-volume,” *Pure Appl. Chem.* **58**, 1239–1248 (1986).

- <sup>28</sup>J. Paczkowski and D. C. Neckers, "Twisted intramolecular charge-transfer phenomenon as a quantitative probe of polymerization kinetics," *Macromolecules* **24**, 3013–3016 (1991).
- <sup>29</sup>P. Bosch, F. Catalina, T. Corrales, and C. Peinado, "Fluorescent probes for sensing processes in polymers," *Chem. Eur. J.* **11**, 4314–4325 (2005).
- <sup>30</sup>D. Antrim, P. Bunton, L. L. Lewis, B. D. Zoltowski, and J. A. Pojman, "Measuring the mutual diffusion coefficient for dodecyl acrylate in low molecular weight poly(dodecyl acrylate) using laser line deflection (Wiener's method) and the fluorescence of pyrene," *J. Phys. Chem. Part B* **109**, 11842–11849 (2005).
- <sup>31</sup>M. Shinitzky, "Membrane fluidity and cellular functions," in *Physiology of Membrane Fluidity*, edited by M. Shinitzky (CRC, Boca Raton, FL, 1984), pp. 1–51.
- <sup>32</sup>M. K. Kuimova, "Mapping viscosity in cells using molecular rotors," *Phys. Chem. Chem. Phys.* **14**, 12671–12686 (2012).
- <sup>33</sup>N. A. Hosny, G. Mohamedi, P. Rademeyer, J. Owen, Y. Wu, M.-X. Tang, R. J. Eckersley, E. Stride, and M. K. Kuimova, "Mapping microbubble viscosity using fluorescence lifetime imaging of molecular rotors," *Proc. Natl. Acad. Sci. U.S.A.* **110**, 9225–9230 (2013).
- <sup>34</sup>A. Mustafic, H.-M. Huang, E. A. Theodorakis, and M. A. Haidekker, "Imaging of flow patterns with fluorescent molecular rotors," *J. Fluoresc.* **20**, 1087–1098 (2010).
- <sup>35</sup>B. Valeur, *Molecular Fluorescence: Principles and Applications* (Wiley-VCH Verlag GmbH, 2001).
- <sup>36</sup>P. Gautam and A. Harriman, "Internal rotation in auramine O," *J. Chem. Soc., Faraday Trans.* **90**, 697–701 (1994).
- <sup>37</sup>M. Y. Berezin and S. Achilefu, "Fluorescence lifetime measurements and biological imaging," *Chem. Rev.* **110**, 2641–2684 (2010).
- <sup>38</sup>T. Atsbeha, A. M. Mohammed, and M. Redi-Abshiro, "Excitation wavelength dependence of dual fluorescence of DMABN in polar solvents," *J. Fluoresc.* **20**, 1241–1248 (2010).
- <sup>39</sup>M. A. Haidekker, M. Nipper, A. Mustafic, D. Lichlyter, M. Dakanali, and E. A. Theodorakis, "Dyes with segmental mobility: Molecular rotors," in *Advanced Fluorescence Reporters in Chemistry and Biology I: Fundamentals and Molecular Design*, Springer Ser Fluoresc Vol. 8, edited by A. P. Demchenko (Springer, 2010), pp. 267–308.
- <sup>40</sup>G. Oster and Y. Nishijima, "Fluorescence and internal rotation: Their dependence on viscosity of the medium," *J. Am. Chem. Soc.* **78**, 1581–1584 (1956).
- <sup>41</sup>J. B. Segur and H. E. Oberstar, "Viscosity of glycerol and its aqueous solutions," *Ind. Eng. Chem.* **43**, 2117–2120 (1951).
- <sup>42</sup>G. M. Homsy, "Viscous fingering in porous media," *Ann. Rev. Fluid Mech.* **19**, 271–311 (1987).
- <sup>43</sup>E. Lajeunesse, J. Martin, N. Rakotomalala, D. Salin, and Y. C. Yortsos, "Miscible displacement in a Hele-Shaw cell at high rates," *J. Fluid Mech.* **398**, 299–319 (1999).
- <sup>44</sup>S. B. Savage, "Laminar radial flow between parallel plates," *J. Appl. Mech.* **31**, 594–596 (1964).
- <sup>45</sup>J. D. Jackson and G. R. Symmons, "An investigation of laminar radial flow between two parallel discs," *Appl. Sci. Res. A* **15**, 59–75 (1965).
- <sup>46</sup>A. F. Elkouh, "Inertia effect in laminar radial flow between parallel plates," *Int. J. Mech. Sci.* **9**, 253–255 (1967).
- <sup>47</sup>G. H. Vatistas, "Radial flow between two closely placed flat disks," *AIAA J.* **26**, 887–889 (1988).
- <sup>48</sup>G. Zitouni and G. H. Vatistas, "Purely accelerating and decelerating flows within two flat disks," *Acta Mech.* **123**, 151–161 (1997).
- <sup>49</sup>W. S. Ghaly and G. H. Vatistas, "Numerical computations of purely radial flow within two concentric disks," *AIAA J.* **39**, 1208–1210 (2001).
- <sup>50</sup>F. Haudin, L. A. Riolfo, B. Knaepen, G. M. Homsy, and A. De Wit, "Experimental study of a buoyancy-driven instability of a miscible horizontal displacement in a Hele-Shaw cell," *Phys. Fluids* **26**, 044102 (2014).